



HAL
open science

A micromechanical model of a hard interface with micro-cracking damage

Maria Letizia Raffa, Frédéric Lebon, Raffaella Rizzoni

► **To cite this version:**

Maria Letizia Raffa, Frédéric Lebon, Raffaella Rizzoni. A micromechanical model of a hard interface with micro-cracking damage. *International Journal of Mechanical Sciences*, 2022, pp.106974. 10.1016/j.ijmecsci.2021.106974 . hal-03404654v2

HAL Id: hal-03404654

<https://hal.science/hal-03404654v2>

Submitted on 15 Jul 2024

HAL is a multi-disciplinary open access archive for the deposit and dissemination of scientific research documents, whether they are published or not. The documents may come from teaching and research institutions in France or abroad, or from public or private research centers.

L'archive ouverte pluridisciplinaire **HAL**, est destinée au dépôt et à la diffusion de documents scientifiques de niveau recherche, publiés ou non, émanant des établissements d'enseignement et de recherche français ou étrangers, des laboratoires publics ou privés.

A micromechanical model of a hard interface with micro-cracking damage

Maria Letizia Raffa^{a,*}, Frédéric Lebon^b, Raffaella Rizzoni^c

^a*Laboratoire QUARTZ, EA 7393, ISAE-Supméca, 3 rue Fernand Hainaut 93407 Saint-Ouen, France*

^b*Aix Marseille Univ, CNRS, Centrale Marseille, LMA, 4 impasse Nikola Tesla 13453 Marseille Cedex 13, France*

^c*Department of Engineering, University of Ferrara, via Saragat 1 44122 Ferrara, Italy*

Abstract

Bonding techniques are increasingly used in many industrial fields. Modelling the under-load damaging behavior of hard structural adhesives is still an open challenge. This work proposes a new hard interface analytical model with evolutive micro-cracking damage. The model is obtained within a rigorous theoretical framework combining asymptotic theory and micromechanical homogenization. Main new features are: (i) the adoption of two dual homogenization approaches; (ii) the formulation of a thermodynamically-based damage evolution law for hard interfaces. The interface model is able to describe both ductile and brittle damage behavior of hard structural adhesives. Provided examples on the structural behavior, under several loads, suggest the suitability of the proposed interface model as a modelling strategy for hard structural adhesives with micro-cracking damage.

*Corresponding author

Email addresses: maria-letizia.raffa@isae-supmeca.fr (Maria Letizia Raffa), lebon@lma.cnrs-mrs.fr (Frédéric Lebon), raffaella.rizzoni@unife.it (Raffaella Rizzoni)

Keywords: bonding, adhesives, damage, imperfect interfaces,
homogenization, asymptotic theory

1 **1. Introduction**

2 Bonding has become a very common practice to assembly materials and
3 structural elements in many industrial fields, such as aeronautic, spatial,
4 automotive, nuclear, civil, mechanical and bio-engineering, mainly because
5 structural adhesives offer low-cost techniques and a great design freedom
6 while preserving good mechanical performances. For some applications, such
7 as assemblies of fiber-reinforced composites and implant fixations, bonding is
8 the only viable assembly technology. To achieve better performances avoiding
9 too large mismatch in terms of thermo-elastic properties, structural adhesives
10 and adherents have, in some cases, an equivalent stiffness. Some examples
11 can be cited: acrylic adhesives, whose Young's modulus (E) is around 2-3
12 GPa [1], are used in manufacture of plywood ($E = 5 - 8$ GPa); phenolic and
13 epoxy adhesives with $E = 3 - 5$ GPa [2] are used to bond structures of GFRP
14 (polyester-glass composites) with $E = 15 - 28$ GPa; orthodontic adhesives
15 with $E = 18 - 22$ GPa [3] are usually used for cementation of brackets on
16 enamel ($E \simeq 65$ GPa).

17 An adhesive equally stiffer than adherents is defined, from a mechani-
18 cal point of view, as a *hard* interface, as opposed to the definition of *soft*
19 interface [4, 5]. A wide literature exists concerning models of soft material
20 interfaces, including those undergoing material degradation. Analytical soft
21 interface models often take into account the nonlinear evolution of the inter-
22 face properties by introducing at least one parameter (of damage, adhesion,

23 etc.) whose variation depends macroscopically on kinematic variables [6–15].
24 Numerical soft interface models, in the framework of the finite element the-
25 ory, generally use cohesive zone models (CZM) based on traction-separation
26 laws of various shapes, to describe cohesive and adhesive failure [16–22].

27 Recently, some analytical models of hard material interfaces have been
28 also developed [23–29] and it has been proved that interface models developed
29 for soft adhesives cannot be directly applied in the case of hard adhesives [25].
30 Moreover, the existing hard interface models do not consider the degradation
31 of the adhesive material properties.

32 This paper provides a novelty within this context, by proposing a hard
33 material interface model accounting for an evolutive micro-cracking damage.
34 In the last twenty years, the present authors established an original modelling
35 strategy to derive soft and hard imperfect interface models based on the
36 combination of asymptotic theory and micromechanical homogenization [11,
37 14, 23–26] (see Fig. 1). This strategy has already been successfully used
38 to describe the mechanics of thin elastic layers in adhesive-like problems
39 and contact problems [13, 15, 30, 31]. Moreover, it has been identified as a
40 sound alternative to the classical cohesive zone models, principally because
41 imperfect interface models allow to consider the physics of the adhesives in
42 terms of geometrical (thickness, surface roughness), mechanical (anisotropy,
43 non-linearity) and damage properties.

44 This work is an extension of the authors’ modelling strategy of hard im-
45 perfect interfaces. Drawing on Kachanov’s micromechanical homogenization
46 theory [32–37], micro-cracking damage is represented by a microcracks den-
47 sity parameter. Particularly, the adoption of a generalized cracks density [38]

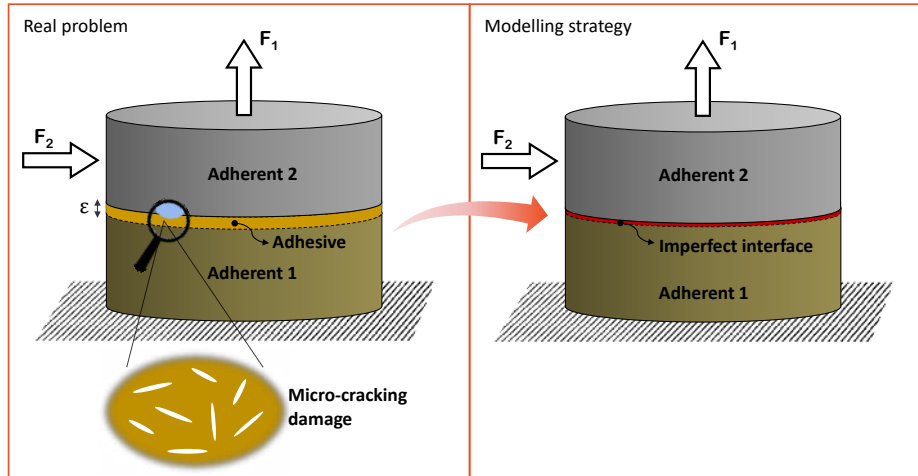


Fig. 1: Schematic sketch of the imperfect interface modelling strategy

48 allows to by-pass the geometrical definition of the cracks, which is possible
 49 only for circular and regular cracks [32], and as a matter of fact it extends the
 50 generality of the proposed interface model to any regular and irregular cracks
 51 shape. It should also be noted that the generalized microcracks density can
 52 be measured *postmortem* by X-ray micro-tomography [15]. The evolutive
 53 character of the micro-cracking damage is described by introducing a new
 54 evolution law of the generalized cracks density.

55 The paper is structured as follows. The hard imperfect interface law is
 56 derived via the asymptotic expansions method in Section 2. In Section 3,
 57 the microcracked-material-interface properties are derived through two dual
 58 approaches of micromechanical homogenization, stress [32, 33] and strain-
 59 based [39, 40]. The damage evolution law is derived from a thermodynamic

60 approach and then included in the hard interface model via the asymptotic
 61 expansions method. In Section 4, the behavior of the proposed interface
 62 model under various loading type is discussed via some academic examples.
 63 Moreover, the influence of damage parameters is investigated. Conclusions
 64 and perspectives are drawn at the end of the paper.

65 **2. Derivation of the hard imperfect interface model**

66 *2.1. Notation and problem statement*

67 The herein adopted matched asymptotic expansion theory builds on the
 68 tradition of using asymptotic analysis to derive mechanical laws governing
 69 imperfect interface conditions [41–48].

70 In what follows, a thin material layer of constant thickness t embedded
 71 between at least two solids is referred as *interphase*. Being L a representa-
 72 tive length scale of the geometry, the non-dimensional interphase thickness
 73 $\varepsilon = t/L$ can be defined and taken as a small parameter for the asymptotic
 74 expansions of the elastic problem. When $\varepsilon \ll 1$, the thin layer can be sub-
 75 stituted by a surface separating the adherents called *interface* across which
 76 certain conditions on the displacements and tractions prevail [4].

77 The interphase occupies a domain \mathcal{B}^ε with cross-section \mathcal{S} , \mathcal{S} being an
 78 open bounded set in \mathbb{R}^2 with a smooth boundary. The *adherents* occupy the
 79 reference configurations $\Omega^\varepsilon_\pm \subset \mathbb{R}^3$. Let $\mathcal{S}^\varepsilon_\pm$ be taken to denote the plane
 80 interfaces between interphase and adherents and let $\Omega^\varepsilon = \Omega^\varepsilon_\pm \cup \mathcal{S}^\varepsilon_\pm \cup \mathcal{B}^\varepsilon$
 81 denote the whole composite system. It is assumed that the displacement and
 82 stress vector fields are continuous across $\mathcal{S}^\varepsilon_\pm$.

83 An orthonormal Cartesian basis $(O, \mathbf{i}_1, \mathbf{i}_2, \mathbf{i}_3)$ is introduced and let (x_1, x_2, x_3)

84 be taken to denote the three coordinates of a particle. The origin of the basis
 85 belongs to \mathcal{S} . The aforementioned system is sketched in Fig. 2a.

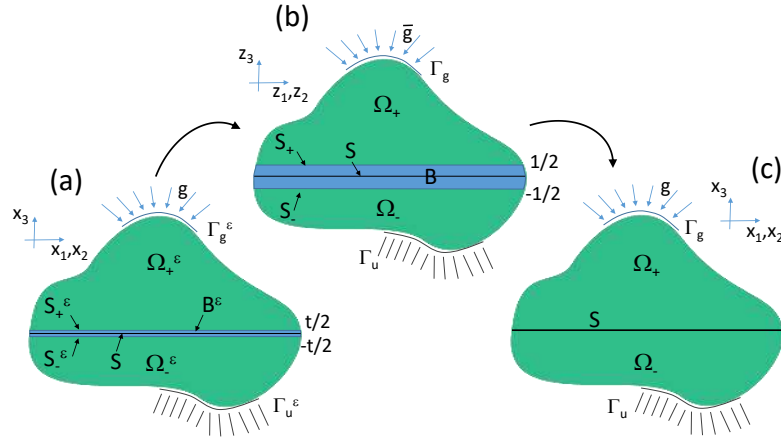


Fig. 2: The three steps of the matched asymptotic expansion method: (a) Reference configuration (interphase); (b) Rescaled configuration (asymptotic expansion phase); (c) Limit configuration (interface).

86 The materials of the composite system are assumed to be homogeneous
 87 and linearly elastic and let $\mathbb{A}_\pm, \mathbb{B}^\epsilon$ be the fourth-rank elasticity tensors of
 88 adherents and of interphase, respectively. Tensors $\mathbb{A}_\pm, \mathbb{B}^\epsilon$ have the usual
 89 symmetry properties, with the minor and major symmetries, and are posi-
 90 tive definite. Note that **any assumption on the anisotropy of adhesive and**
 91 **adherents materials is needed for the proposed development. As a matter of**
 92 **fact, it extends the generality of the proposed asymptotic approach to any**
 93 **anisotropic material.**

94 Adherents are subjected to a body force density $\mathbf{f}^\pm : \Omega^\epsilon_\pm \mapsto \mathbb{R}^3$ and to a
 95 surface force density $\mathbf{g}^\pm : \Gamma_g^\epsilon \mapsto \mathbb{R}^3$ on $\Gamma_g^\epsilon \subset (\partial\Omega^\epsilon_+ \setminus \mathcal{S}_+^\epsilon) \cup (\partial\Omega^\epsilon_- \setminus \mathcal{S}_-^\epsilon)$. Body

96 forces in the interphase are neglected.

97 On $\Gamma_u^\varepsilon = (\partial\Omega^+ \setminus \mathcal{S}_+^\varepsilon) \cup (\partial\Omega^- \setminus \mathcal{S}_-^\varepsilon) \setminus \Gamma_g^\varepsilon$, homogeneous boundary conditions
98 are prescribed:

$$\mathbf{u}^\varepsilon = \mathbf{0} \quad \text{on } \Gamma_u^\varepsilon, \quad (1)$$

99 where $\mathbf{u}^\varepsilon : \Omega^\varepsilon \mapsto \mathbb{R}^3$ is the displacement field defined on Ω^ε . Boundaries
100 Γ_g^ε , Γ_u^ε are assumed to be located sufficiently far from the interphase and the
101 external boundaries of the interphase \mathcal{B}^ε ($\partial\mathcal{S} \times (-\frac{\varepsilon}{2}, \frac{\varepsilon}{2})$) are assumed to be
102 stress-free. The external forces field is endowed with sufficient regularity to
103 ensure the existence of an equilibrium configuration [25].

104 **The following** notation is adopted:

- 105 • $[f] := f(\mathbf{z}_\alpha, \frac{1}{2}) - f(\mathbf{z}_\alpha, -\frac{1}{2}) \Rightarrow$ jump in the rescaled configuration (Fig. 2b);
- 106 • $\langle f \rangle := \int_{-\frac{1}{2}}^{\frac{1}{2}} f(\mathbf{z}_\alpha, z_3) dz_3 \Rightarrow$ average in the rescaled configuration;
- 107 • $[[f]] := f(\mathbf{x}_\alpha, 0^+) - f(\mathbf{x}_\alpha, 0^-) \Rightarrow$ jump in the limit configuration (Fig. 2c);
- 108 • $\langle\langle f \rangle\rangle := \frac{1}{2}(f(\mathbf{x}_\alpha, 0^+) + f(\mathbf{x}_\alpha, 0^-)) \Rightarrow$ average in the limit configuration;

109 where f is a generic function, $\mathbf{z}_\alpha = (z_1, z_2)$ and $\mathbf{x}_\alpha = (x_1, x_2)$.

110 2.2. The one-order asymptotic theory

111 This section details the main steps of the asymptotic analysis leading to
112 the hard interface law at one-order. Full formulation is reported in Appendix
113 A and more details could be found in [23–26].

114 **Generally, the elasticity tensor \mathbb{B}^ε of a hard interphase does not depend**
115 **on ε [23, 25]:**

$$\mathbb{B}^\varepsilon = \mathbb{B} \quad (2)$$

116 In the rescaled configuration (Fig. 2b) and **considering** Eqs. (A.7) and
 117 (A.14b), the stress-strain equation (A.31b) reads as:

$$\hat{\boldsymbol{\sigma}}^0 + \varepsilon \hat{\boldsymbol{\sigma}}^1 = \mathbb{B}(\varepsilon^{-1} \hat{\mathbf{e}}^{-1} + \hat{\mathbf{e}}^0 + \varepsilon \hat{\mathbf{e}}^1) + o(\varepsilon) \quad (3)$$

Equation (3) is true $\forall \varepsilon$, thus the following conditions are derived:

$$\mathbf{0} = \mathbb{B}(\hat{\mathbf{e}}^{-1}) \quad (4a)$$

$$\hat{\boldsymbol{\sigma}}^0 = \mathbb{B}(\hat{\mathbf{e}}^0) \quad (4b)$$

118 **By considering** Eq. (A.8) and the positive definiteness of the tensor \mathbb{B} , Eq. (4a)
 119 gives:

$$\hat{\mathbf{u}}_{,3}^0 = 0 \Rightarrow [\hat{\mathbf{u}}^0] = \mathbf{0} \quad (5)$$

120 **Moreover**, substituting Eq. (A.9) written for $k = 0$ into Eq. (4b) **it** gives:

$$\hat{\boldsymbol{\sigma}}^0 \mathbf{i}_j = \mathbf{K}^{1j} \hat{\mathbf{u}}_{,1}^0 + \mathbf{K}^{2j} \hat{\mathbf{u}}_{,2}^0 + \mathbf{K}^{3j} \hat{\mathbf{u}}_{,3}^1 \quad (6)$$

121 with $j = 1, 2, 3$ and \mathbf{K}^{jl} being the two-order tensors such that $K_{ki}^{jl} := B_{ijkl}$.

122 **Next**, integrating Eq. (6) with respect to z_3 (for $j = 3$) and considering
 123 Eq. (A.17) it results:

$$[\hat{\mathbf{u}}^1] = (\mathbf{K}^{33})^{-1} (\hat{\boldsymbol{\sigma}}^0 \mathbf{i}_3 - \mathbf{K}^{\alpha 3} \hat{\mathbf{u}}_{,\alpha}^0) \quad (7)$$

124 **Then**, by replacing Eq. (6) ($j = 1, 2$) **in the equilibrium equation (A.18) one**
 125 **obtains:**

$$(\hat{\boldsymbol{\sigma}}^1 \mathbf{i}_3)_{,3} = -(\hat{\boldsymbol{\sigma}}^0 \mathbf{i}_\alpha)_{,\alpha} = -(\mathbf{K}^{1\alpha} \hat{\mathbf{u}}_{,1}^0 + \mathbf{K}^{2\alpha} \hat{\mathbf{u}}_{,2}^0 + \mathbf{K}^{3\alpha} \hat{\mathbf{u}}_{,3}^1)_{,\alpha} \quad (8)$$

126 **Next**, by integrating Eq. (8) with respect to z_3 between $-1/2$ and $1/2$ and
 127 by using Eq. (7), it is obtained:

$$[\hat{\boldsymbol{\sigma}}^1 \mathbf{i}_3] = \left(-\mathbf{K}^{\beta\alpha} \hat{\mathbf{u}}_{,\beta}^0 - \mathbf{K}^{3\alpha} (\mathbf{K}^{33})^{-1} (\hat{\boldsymbol{\sigma}}^0 \mathbf{i}_3 - \mathbf{K}^{\beta 3} \hat{\mathbf{u}}_{,\beta}^0) \right)_{,\alpha} \quad (9)$$

128 where Greek indexes ($\alpha, \beta = 1, 2$) are related to the in-plane (x_1, x_2) quan-
 129 tities. Note that in Eq. (9) higher order effects, related to in-plane deriva-
 130 tives, appear. These terms, usually neglected in standard zero-order theories
 131 [23, 25], are related to the curvature of the deformed interface (second-order
 132 derivatives).

133 Finally, the transition from the rescaled configuration to the limit configura-
 134 tion is obtained by introducing the matching conditions Eqs.(A.27)-(A.30)
 135 and the interface laws at both zero-order and one-order are derived:

- Zero-order interface law:

$$[[\mathbf{u}^0]] = \mathbf{0} \quad (10)$$

$$[[\boldsymbol{\sigma}^0 \mathbf{i}_3]] = \mathbf{0} \quad (11)$$

- One-order interface law:

$$[[\mathbf{u}^1]] = (\mathbf{K}^{33})^{-1} (\boldsymbol{\sigma}^0 \mathbf{i}_3 - \mathbf{K}^{\alpha 3} \mathbf{u}_{,\alpha}^0) - \langle\langle \mathbf{u}_{,3}^0 \rangle\rangle \quad (12)$$

$$[[\boldsymbol{\sigma}^1 \mathbf{i}_3]] = \left(-\mathbf{K}^{\beta \alpha} \mathbf{u}_{,\beta}^0 - \mathbf{K}^{3\alpha} (\mathbf{K}^{33})^{-1} (\boldsymbol{\sigma}^0 \mathbf{i}_3 - \mathbf{K}^{\beta 3} \mathbf{u}_{,\beta}^0) \right)_{,\alpha} \\ - \langle\langle \boldsymbol{\sigma}_{,3}^0 \mathbf{i}_3 \rangle\rangle \quad (13)$$

136 Equations (10)-(11) are the standard perfect interface condition, character-
 137 ized by the continuity in terms of displacements and stresses at the interface
 138 [4]. Equations (12)-(13) are the displacements and stresses jumps at the inter-
 139 face in the one-order asymptotic theory. They depend on the displacements
 140 and the stresses fields at the zero-order and on their first and second-order
 141 derivatives.

142 The hard interface law in the reference configuration (Fig.2a) is derived by
 143 considering **asymptotic** expansions (A.14a) and (A.5a) combined with Eqs.
 144 (10)-(13) [25]:

$$[[\mathbf{u}^\varepsilon]] \approx \varepsilon \left((\mathbf{K}^{33})^{-1} (\langle\langle \boldsymbol{\sigma}^\varepsilon \mathbf{i}_3 \rangle\rangle - \mathbf{K}^{\alpha 3} \langle\langle \mathbf{u}_{,\alpha}^\varepsilon \rangle\rangle) - \langle\langle \mathbf{u}_{,3}^\varepsilon \rangle\rangle \right) \quad (14)$$

$$[[\boldsymbol{\sigma}^\varepsilon \mathbf{i}_3]] \approx \varepsilon \left(\left(-\mathbf{K}^{\beta\alpha} \langle\langle \mathbf{u}_{,\beta}^\varepsilon \rangle\rangle - \mathbf{K}^{3\alpha} (\mathbf{K}^{33})^{-1} (\langle\langle \boldsymbol{\sigma}^\varepsilon \mathbf{i}_3 \rangle\rangle - \mathbf{K}^{\beta 3} \langle\langle \mathbf{u}_{,\beta}^\varepsilon \rangle\rangle) \right)_{,\alpha} \right. \\ \left. - \langle\langle \boldsymbol{\sigma}_{,3}^\varepsilon \mathbf{i}_3 \rangle\rangle \right) \quad (15)$$

145 **3. Introduction of the micro-cracking damage**

146 In this section, it is shown how to include micro-cracking damage in the
 147 hard interface law above obtained. The closed-form of the effective elastic
 148 tensors \mathbf{K}^{jl} in Eqs. (14)-(15) is specialized by using micromechanical ho-
 149 mogenization in the case of two microcracked material models: Kachanov-
 150 Sevostianov (KS) and Welemane-Goidescu (WG) models. The evolution law
 151 of the **generalized** microcracks density is derived from a **thermodynamic ap-
 152 proach** and then included in the hard interface model via the asymptotic
 153 expansions method.

154 *3.1. Micromechanical homogenization approaches*

155 The Kachanov-Sevostianov model [32, 37] is a stress-based approach based
 156 on the non-interacting microcracks approximation [35, 36]. The Welemane-
 157 Goidescu model [40, 49, 50] is a strain-based approach, based on **the** dilute
 158 limit hypothesis [39]. For both models, it is assumed that the material in-
 159 terphase comprises an orthotropic matrix embedding a family of microcracks
 160 parallel to \mathbf{i}_1 . For the sake of simplicity, the formulations are reduced to

161 the two-dimensional case on the plane ($\mathbf{i}_1, \mathbf{i}_3$) with reference to the problem
 162 geometry in Fig.2.

163 3.1.1. Kachanov-Sevostianov model

164 Following the theory proposed by Kachanov and coworkers [32–37] based
 165 on the Eshelby’s approach [51], and the above assumptions on microcracks
 166 and matrix, the interface stiffness can be derived as follows:

$$\begin{aligned}
 K_{11}^{11} &= \frac{(E_1^0)^2 (2 R B_{nn} E_3^0 + 1)}{E_1^0 - E_3^0 (\nu_{13}^0)^2 + 2 R B_{nn} E_1^0 E_3^0} \\
 K_{31}^{13} &= K_{13}^{31} = \frac{E_1^0 E_3^0 \nu_{13}^0}{E_1^0 - E_3^0 (\nu_{13}^0)^2 + 2 R B_{nn} E_1^0 E_3^0} \\
 K_{33}^{33} &= \frac{E_1^0 E_3^0}{E_1^0 - E_3^0 (\nu_{13}^0)^2 + 2 R B_{nn} E_1^0 E_3^0} \\
 K_{11}^{33} &= \frac{2 G_{13}^0}{2 + R B_{tt} G_{13}^0}
 \end{aligned} \tag{16}$$

167 where $E_1^0, E_3^0, G_{13}^0, \nu_{13}^0$ and ν_{31}^0 are the in-plane elastic orthotropic moduli of
 168 the matrix; B_{nn} and B_{tt} are elastic parameters depending on the matrix and
 169 microcracks characteristics [32, 33].

170 Note that the engineering moduli can be also easily derived. The effective
 171 Young’s modulus in normal direction (\mathbf{i}_3), used in the examples below, reads
 172 as:

$$E_3 = \frac{E_3^0}{1 + 2 R B_{nn} E_3^0} \tag{17}$$

173 3.1.2. Welemane-Goidescu model

174 In [40, 49, 50, 52], Welemane and coworkers extended the energy-based
 175 homogenization approach originally proposed in [39] for isotropic materials
 176 to the case of an orthotropic matrix.

177 By following the Welemane-Goidescu model [49], the expressions of the
178 interface stiffness read as:

$$\begin{aligned}
K_{11}^{11} &= \frac{E_1^0}{E_3^0(\nu_{13}^0\nu_{31}^0 - 1)^2} \left(E_3^0(1 - \nu_{13}^0\nu_{31}^0) - R\sqrt{E_3^0}(\nu_{31}^0)^2\pi\chi \right) \\
K_{31}^{13} &= K_{13}^{31} = \frac{E_1^0\nu_{31}^0}{(\nu_{13}^0\nu_{31}^0 - 1)^2} \left((1 - \nu_{13}^0\nu_{31}^0) - R\sqrt{E_3^0}\pi\chi \right) \\
K_{33}^{33} &= \frac{E_3^0}{(\nu_{13}^0\nu_{31}^0 - 1)^2} \left((1 - \nu_{13}^0\nu_{31}^0) - R\sqrt{E_3^0}\pi\chi \right) \\
K_{11}^{33} &= G_{13}^0 \left(1 - R\frac{\pi}{\sqrt{E_1^0}}G_{13}^0\chi \right)
\end{aligned} \tag{18}$$

179 where $\chi = \left(\frac{1}{G_{13}^0} - 2\frac{\nu_{13}^0}{E_1^0} + \frac{2}{\sqrt{E_1^0E_3^0}} \right)^{\frac{1}{2}}$, and E_1^0 , E_3^0 , G_{13}^0 , ν_{13}^0 and ν_{31}^0 are the
180 in-plane elastic orthotropic moduli of the matrix.

181 Also in this case, the engineering moduli can be derived. The effective
182 Young's modulus in normal direction (\mathbf{i}_3), adopted for next examples below,
183 reads as:

$$E_3 = E_3^0 (1 - 2RH_{nn}E_3^0) \tag{19}$$

184 with H_{nn} an elastic parameter depending on the matrix and microcracks
185 characteristics [49] (analogous to the parameter B_{nn} of the KS model).

186 3.2. Damage evolution law

187 The proposed hard interface law expressed by Eqs. (12)-(13) in the limit
188 configuration (Fig. 2c), or by Eqs. (14)-(15) in the reference configuration
189 (Fig. 2a), depends on the generalized microcracks density R via the effective
190 stiffness tensors expressed by Eqs. (16) and Eqs. (18) for the KS and WG
191 model, respectively.

192 A possible evolution law of R in the interphase \mathcal{B}^ε (of thickness ε) is herein
193 derived following a thermodynamic approach [6, 7]. A pseudo-potential of

194 dissipation Φ given by the sum of a quadratic term and a positively 1-
 195 homogeneous functional is considered [7]. The dissipative character of the
 196 evolution of damage is given by the rate-dependent form of the potential:

$$\Phi(\dot{R}) = \frac{1}{2} \eta^\varepsilon \dot{R}^2 + I_{[0,+\infty[}(\dot{R}), \quad (20)$$

197 where η^ε is a positive viscosity parameter; $I_{\mathcal{A}}$ denotes the indicator function
 198 of the set \mathcal{A} , i.e. $I_{\mathcal{A}}(x) = 0$ if $x \in \mathcal{A}$ and $I_{\mathcal{A}}(x) = +\infty$ otherwise; \dot{R} is the
 199 increment of microcracks density compared to its initial level, indicated in
 200 what follows as R_0 . The term $I_{[0,+\infty[}(\dot{R})$ forces \dot{R} to assume non-negative
 201 values and it gives the irreversible character of the degradation process for a
 202 non-regenerative microcracked material ($R \geq R_0$).

203 The free energy associated with the constitutive equation of the micro-
 204 racked material is chosen as follows:

$$\Psi(\mathbf{e}(\mathbf{u}^\varepsilon), R) = \frac{1}{2} \mathbb{B}^\varepsilon(R) (\mathbf{e}(\mathbf{u}^\varepsilon) : \mathbf{e}(\mathbf{u}^\varepsilon)) - \omega^\varepsilon R + I_{[R_0,+\infty[}(R) \quad (21)$$

205 where $\mathbb{B}^\varepsilon(R)$ is the effective stiffness tensor of the material (obtained via the
 206 KS or WG model); \mathbf{u} is the displacement field; $\mathbf{e}(\mathbf{u})$ is the strain tensor under
 207 the small perturbation hypothesis; ω^ε is a strictly negative parameter. Note
 208 that the irreversible character of damage, already imposed in Eq. (20), allows
 209 to neglect the term $I_{[R_0,+\infty[}(R)$ in Eq. (21).

210 By deriving Eqs. (20) and (21) with respect \dot{R} and R respectively, then
 211 by replacing them into the movement equations in \mathcal{B}^ε (for further details
 212 refer to [6, 53]), the following damage evolution law for \dot{R} in the volume \mathcal{B}^ε
 213 is obtained:

$$\eta^\varepsilon \dot{R} = \left(\omega^\varepsilon - \frac{1}{2} \mathbb{B}_{,R}^\varepsilon(R) (\mathbf{e}(\mathbf{u}^\varepsilon) : \mathbf{e}(\mathbf{u}^\varepsilon)) \right)_+ \quad (22)$$

214 where $(\cdot)_+$ denotes the positive part of the function and $\mathbb{B}_{,R}^\varepsilon(R)$ indicates
 215 the component-wise derivative of the stiffness tensor with respect to the
 216 **generalized** microcracks density R .

217 3.2.1. Asymptotic theory

218 In this section, the asymptotic behavior of **the volumetric damage evolu-**
 219 **tion law (Eq. (22))** is studied. It is prescribed that η^ε and ω^ε are volumetric
 220 densities and thus they are inversely proportional to the non-dimensional
 221 interphase thickness ε : $\eta^\varepsilon = \eta \varepsilon^{-1}$ and $\omega^\varepsilon = \omega \varepsilon^{-1}$, with $\eta > 0$ and $\omega < 0$.
 222 Subsequently, for the sake of simplicity, we will further assume that ω and η
 223 do not depend on the direction orthogonal to the interface surface x_3 (respec-
 224 tively z_3 , in the rescaled configuration). **In the following, also** R is supposed
 225 to be independent of x_3 (respectively z_3).

226 Let focus on the term: $\frac{1}{2} \mathbb{B}_{,R}^\varepsilon(R) (\mathbf{e}(\mathbf{u}^\varepsilon) : \mathbf{e}(\mathbf{u}^\varepsilon))$ in Eq. (22). This term can
 227 be developed at 0-order as $\frac{1}{2} \mathbb{B}_{,R}^\varepsilon(R) (\hat{\mathbf{e}}^0 : \hat{\mathbf{e}}^0)$, and the constitutive equation
 228 (4b) leads to $\frac{1}{2} \mathbb{B}_{,R}^\varepsilon(R) [(\mathbb{B}^\varepsilon)^{-1}(R) \hat{\sigma}^0 : \hat{\mathbf{e}}^0]$. Note that:

$$\hat{\mathbf{e}}^0 = Sym(\hat{u}_{,1}^0 \otimes i_1 + \hat{u}_{,2}^0 \otimes i_2 + \hat{u}_{,3}^1 \otimes i_3) \quad (23)$$

229 where Sym gives the symmetric part of the enclosed tensor. This term is inte-
 230 grated along z_3 and gives $\frac{1}{2} \mathbb{B}_{,R}^\varepsilon(R) [(\mathbb{B}^\varepsilon)^{-1}(R) \hat{\sigma}^0 : \langle \hat{\mathbf{e}}^0 \rangle]$ or $\frac{1}{2} \mathbb{B}_{,R}^\varepsilon(R) (\hat{\mathbf{e}}^0 : \langle \hat{\mathbf{e}}^0 \rangle)$.
 231 **Next, by** integrating again along z_3 , it gives $\frac{1}{2} \mathbb{B}_{,R}^\varepsilon(R) (\langle \hat{\mathbf{e}}^0 \rangle : \langle \hat{\mathbf{e}}^0 \rangle)$, where

$$\langle \hat{\mathbf{e}}^0 \rangle = Sym(\hat{u}_{,1}^0 \otimes i_1 + \hat{u}_{,2}^0 \otimes i_2 + [\hat{u}^1] \otimes i_3) \quad (24)$$

232 **Finally, by adopting the following approximation:**

$$Sym(\hat{u}_{,1}^0 \otimes i_1 + \hat{u}_{,2}^0 \otimes i_2 + [\hat{u}^1] \otimes i_3) \approx Sym(\hat{u}_{,1}^\varepsilon \otimes i_1 + \hat{u}_{,2}^\varepsilon \otimes i_2 + \frac{1}{\varepsilon} [\hat{u}^\varepsilon] \otimes i_3) \quad (25)$$

233 the (internal) damage evolution equation reads:

$$\eta\dot{R} = \left\{ \omega - \frac{1}{2} K_{,R}^\varepsilon(R) \begin{pmatrix} \langle u_{,1}^\varepsilon \rangle \\ \langle \hat{u}_{,2}^\varepsilon \rangle \\ [\hat{u}^\varepsilon] \end{pmatrix} \cdot \begin{pmatrix} \langle \hat{u}_{,1}^\varepsilon \rangle \\ \langle \hat{u}_{,2}^\varepsilon \rangle \\ [\hat{u}^\varepsilon] \end{pmatrix} \right\}_+ \quad (26)$$

where

$$K^\varepsilon = \begin{pmatrix} \varepsilon K^{11} & \varepsilon K^{12} & K^{13} \\ \varepsilon K^{12} & \varepsilon K^{22} & K^{23} \\ K^{13} & K^{23} & \frac{1}{\varepsilon} K^{33} \end{pmatrix}$$

234 By introducing the matching conditions of the hard interface law (Eqs. (14)-
 235 (15)) and neglecting the second-order terms, the final form of the proposed
 236 damage evolution law for a hard interface model reads:

$$\eta\dot{R} = \left\{ \omega - \frac{1}{2} K_{,R}(R) \begin{pmatrix} \langle\langle u_{,1}^\varepsilon \rangle\rangle \\ \langle\langle u_{,2}^\varepsilon \rangle\rangle \\ [[u^\varepsilon]] + \varepsilon \langle\langle u_{,3}^\varepsilon \rangle\rangle \end{pmatrix} \cdot \begin{pmatrix} \langle\langle u_{,1}^\varepsilon \rangle\rangle \\ \langle\langle u_{,2}^\varepsilon \rangle\rangle \\ [[u^\varepsilon]] + \varepsilon \langle\langle u_{,3}^\varepsilon \rangle\rangle \end{pmatrix} \right\}_+ \quad (27)$$

237

238 3.3. Connection of the generalized cracks density with normalized damage 239 parameters

240 In the classical continuum damage theory at least one normalized damage
 241 variable is adopted to describe non-localized damage [6, 53, 54]. The simplest
 242 relationship to describe material properties degradation is $E = E^0(1 - D)$,
 243 where E^0 is the Young's modulus of the undamaged material and D is the
 244 damage variable going from 0 in undamaged conditions to 1 in fully damaged
 245 conditions. This damage description is generally used in commercial software
 246 for finite element analysis (FEA). Connection relationships between D and

247 the generalized cracks density R can be obtained for both KS and WG model
 248 by using Eq.(17) and Eq.(19), respectively, and they read as:

$$\begin{aligned}
 D &= \frac{2 R B_{nn} E^0}{1 + 2 R B_{nn} E^0} && \text{for KS model} \\
 D &= 2 R H_{nn} E^0 && \text{for WG model}
 \end{aligned}
 \tag{28}$$

249 Equations (28) show that in undamaged conditions $D = R = 0$ for both
 250 damaged-material models. Instead, in fully damaged conditions ($D = 1$),
 251 $R \rightarrow +\infty$ for the KS model and it is bounded by the value $R = 1/2 H_{nn} E^0$
 252 for the WG model. Note that to have an upper bound for R , in the WG
 253 model, is consistent with the dilute limit theory, on which the WG model is
 254 based [40], meaning that the model is valid for small density values. These
 255 connection relationships (28) have a twofold advantage: (i) they allow a
 256 microstructural interpretation of the damage variable D , by making explicit
 257 its dependency on material and microcracks properties; (ii) they are expected
 258 to simplify the implementation of the proposed interface model in commercial
 259 FEA-software for future validation with numerical simulation.

260 4. Numerical examples

261 Hereafter, two academic examples are used to illustrate the constitutive
 262 and structural behavior of the proposed hard interface model with micro-
 263 cracking damage. All the numerical computations have been carried out
 264 using the commercial software *Mathematica* [55].

265 4.1. 0-D example: The constitutive behavior

266 In this section, a 0-D example is developed to illustrate the constitutive
 267 behavior of the interface model. Different points are discussed: the compari-

268 son between damaged material models KS and WG; the influence of damage
 269 parameters η and ω on the interface law; and finally, the influence of the
 270 loading rate and of cyclic loads on the interface behavior.

271 4.1.1. Effects of the damage evolution law

272 The mechanical properties of the damaged material (Young's modulus
 273 $E_d(E_u, R)$) in the case of KS (Eq. (17)) and WG (Eq. (19)) models, read as
 274 follows:

$$\begin{aligned} E_d^{KS}(E_u, R) &= \frac{E_u}{1 + 2\pi R} \quad \text{for KS model} \\ E_d^{WG}(E_u, R) &= E_u (1 - 2\pi R) \quad \text{for WG model} \end{aligned} \quad (29)$$

275 where $B_{nn} = H_{nn} = \frac{\pi}{E_u}$. By deriving with respect R , one obtains:

$$\begin{aligned} (E_d^{KS})_{,R} &= -\frac{2\pi E_u}{(1 + 2\pi R)^2} \quad \text{for KS model} \\ (E_d^{WG})_{,R} &= -2\pi E_u \quad \text{for WG model} \end{aligned} \quad (30)$$

276 The damage evolution laws in the 0-D case, for both KS and WG models,
 277 are obtained **substituting Eqs. (30) into Eq. (27)**:

$$\eta \dot{R} = \begin{cases} \left(\omega - \frac{1}{2} \frac{(E_d^{KS})_{,R}}{\varepsilon} [u]_n^2 \right)_+ & \text{for KS model} \\ \left(\omega - \frac{1}{2} \frac{(E_d^{WG})_{,R}}{\varepsilon} [u]_n^2 \right)_+ & \text{for WG model} \end{cases} \quad (31)$$

278 Equations (31) have been numerically solved with an imposed displacement
 279 jump equal to $[u]_n = [u]_{max} \frac{t}{t_f}$ with $[u]_{max} = 0.1$ mm and $t_f = 5$ s. Note that
 280 the time unit (s) is only qualitative and the proposed model does not depend
 281 on it because the interface model is developed in a quasi-static framework.
 282 Moreover, let $E_u = 70 \times 10^3$ MPa and $\varepsilon = 2$ mm. The chosen reference
 283 values for damage parameters are $\eta = 30$ MJ.s/mm² and $\omega = -2$ MJ/mm².
 284 Initial damage was imposed to **vanish** ($R_0 = 0$). To investigate the effects

285 of parameters η and ω on the interface model, a one-factor-a-time (OFAT)
 286 study on both η and ω has been made on ranges $\eta = (0.3, 3, 30, 300)$ and
 287 $\omega = (-0.2, -2, -20, -200)$.

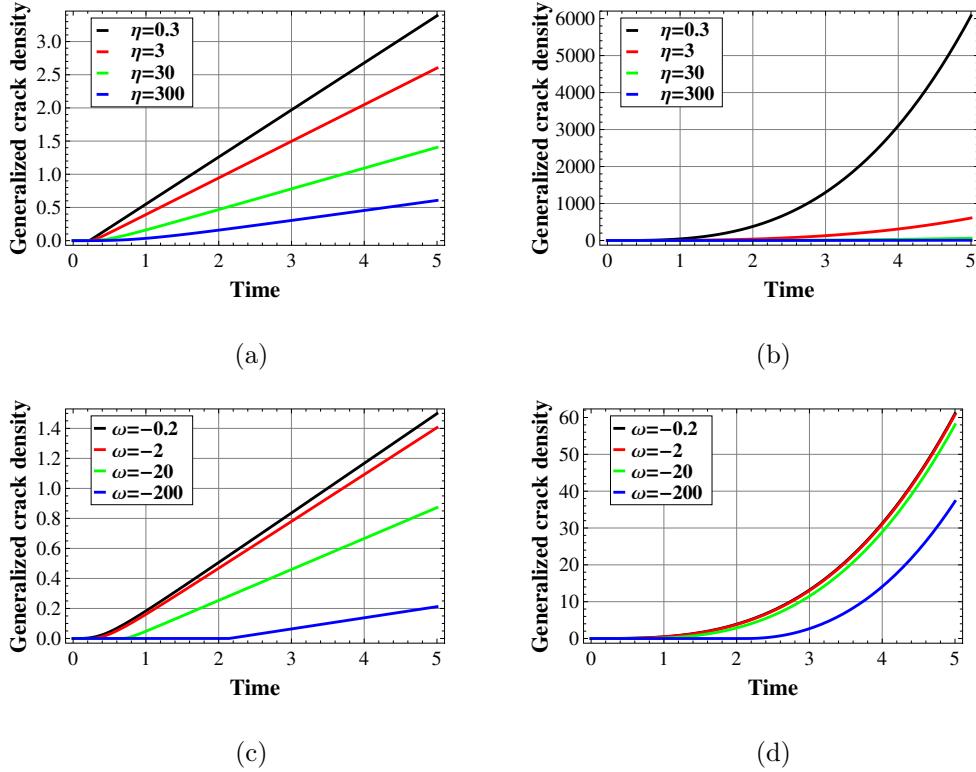


Fig. 3: Evolution of the generalized microcracks density R . Fig. 3(a): effect of varying η in the KS model. Fig. 3(b): effect of varying η in the WG model. Fig. 3(c): effect of varying ω in the KS model. Fig. 3(d): effect of varying ω in the WG model.

288 Figures 3a-d show the evolution of the generalized microcracks density
 289 R as a function of the time and of damage parameters η and ω , for both
 290 KS and WG models. At the beginning, both models present an horizontal

291 plateau at zero (because of the imposed initial damage $R_0 = 0$); then, after
 292 damage initiation, a linear increasing behavior is found for the KS model and
 293 a cubic increasing behavior for the WG model. An inverse proportionality
 294 between R and η is found in both models (see Fig. 3(a) and Fig. 3(b)); this
 295 highlights that η has the physical meaning of a damage viscosity influencing
 296 the velocity (slope of (R, t) curves) of the damage evolution. This result is
 297 also emphasized in Fig. 4, where the degradation of the Young's modulus
 298 of both damaged materials KS and WG is shown. The slope of $(E_d/E_u, t)$
 299 curves, for both KS and WG models, increases as η decreases, meaning that
 300 material get damaged "faster" for smaller values of η .

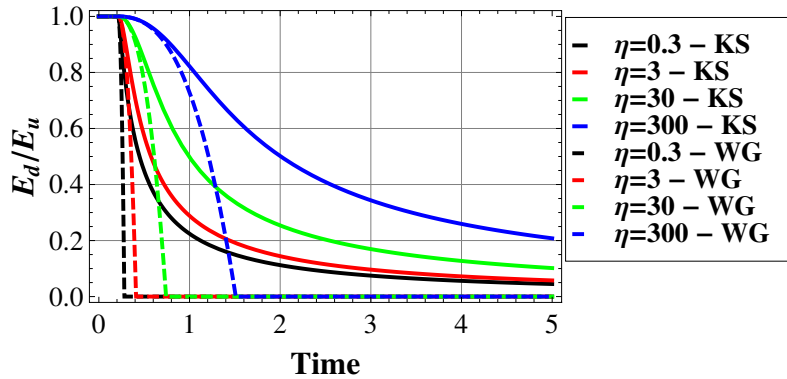


Fig. 4: Evolution in time of the Young's modulus of the damaged materials: parametric study on η . Kachanov-Sevostianov (KS, solid lines) and Welemane-Goidescu (WG, dashed lines) damaged material models are represented.

301 The parameter ω has the physical meaning of a threshold energy beyond
 302 which damage initiate, in analogy with Dupré's energy for adhesion [53]. In
 303 fact, the damage-initiation time, *i.e.*, when R begins to increase, is more

304 influenced by ω than by η for both damaged materials, as highlighted in
 Figs. 3(c), 3(d) and 5.

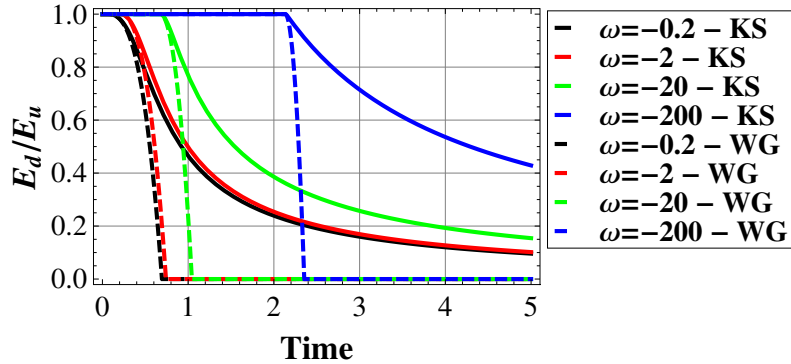


Fig. 5: Evolution in time of the Young's modulus of the damaged materials: parametric study on ω . Kachanov-Sevostianov model (KS, solid lines) and Welemane-Goidescu model (WG, dashed lines).

305

306 Moreover, Figs. 4 and 5 show that the complete damage (*i.e.*, when E_d
 307 tends to zero) occurs earlier for the WG model than for the KS model inde-
 308 pendently of ω and η . Note that in the case of KS model, E_d tends to zero
 309 asymptotically (data not shown). This different behavior of the two models is
 310 consistent with the two different hypotheses on which the models are based.
 311 Particularly, WG model is based on the dilute limit hypothesis, meaning that
 312 it is valid for small density values (less than 20% according to [39]). This is
 313 also in agreement with the fact that the generalized cracks density R has an
 314 upper bound in the case of WG model (see Section 3.3). The KS model is
 315 based on the non-interacting microcracks approximation and it is valid for
 316 greater microcracks densities (until 80% according to [36, 37]). For further

317 details regarding the difference between these microstructural hypotheses the
 318 reader can refer to [37].

319 The interface model in 0-D can be expressed as:

$$\sigma_n = \frac{E_d}{\varepsilon} [u]_n \quad (32)$$

320 Equation (32) has been solved for both KS and WG models, replacing E_d by
 321 E_d^{KS} and E_d^{WG} , respectively (see Eqs. (29)), in which R has been obtained
 by Eqs. (31).

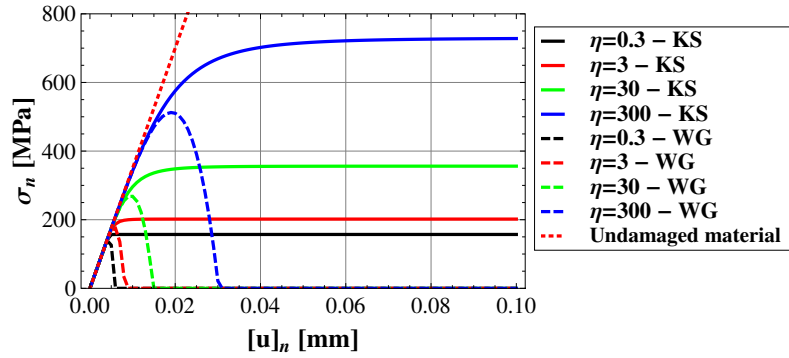


Fig. 6: Interface law: parametric study on η . Kachanov-Sevostianov (KS, solid lines) and Welemanc-Goidescu (WG, dashed lines) damaged material models are represented. The linear-elastic behavior of the undamaged material is represented with a red dotted line.

322

323 Figures 6 and 7 show the interface model for both damaged materials as a
 324 function of η and ω . Numerical curves are obtained by solving the damaged
 325 interface model (Eqs. (32), (29), and (31)) in displacement-controlled mode.
 326 Both figures suggest a brittle damage behavior in the case of WG model and
 327 a ductile damage behavior for the KS model. Figure 6 highlights that the

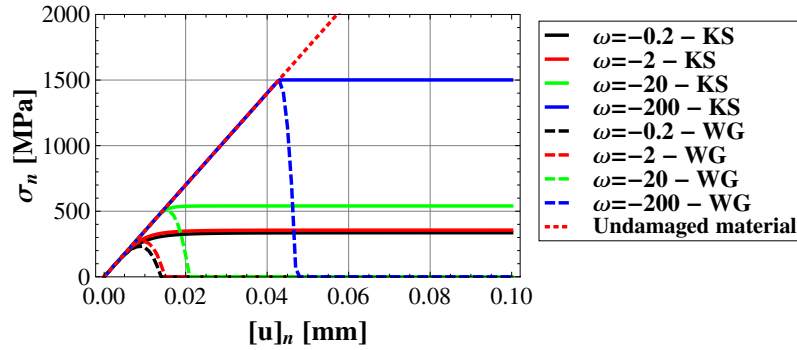


Fig. 7: Interface law: parametric study on ω . Kachanov-Sevostianov (KS, solid lines) and Welemane-Goidescu (WG, dashed lines) damaged material models are represented. The linear-elastic behavior of the undamaged material is represented with a red dotted line.

328 elastic limit increases with η and this result confirms the role of the damage
 329 viscosity η as the velocity of the damage evolution. Figure 6 shows also that η
 330 influences the nonlinear transition between the linear elastic domain and the
 331 damaged domain (this is more evident in **KS model** than in **WG model**); thus
 332 for a small damage viscosity η this transition tends to vanish (*i.e.*, suggesting
 333 that the material gets damaged immediately after the initiation). Figure 7
 334 emphasizes the role of parameter ω as a damage initiation threshold: thus
 335 the higher is ω , the later damage initiates (see Fig. 5) and the higher the
 336 elastic limit.

337 4.1.2. Effects of the loading rate

338 The influence of the loading rate and of the loading shape on the interface
 339 model has been investigated. In particular, two displacement jumps have

340 been separately imposed to solve Eqs. (32), (29), and (31): a ramp function
 341 $[u]_n = v t$ and a quadratic function $[u]_n = 1/2 v^2 t^2 + 1/2 v t$. Four values of the
 342 loading rate $v = [u]_{max} / t_f$ have been simulated (0.1, 0.2, 2, 20) mm/s with a
 343 fixed $[u]_{max} = 1$ mm and by varying the duration t_f between (0.05, 0.5, 5, 10)
 344 s. The damage parameters have been taken equal to their reference values
 345 $\eta = 30$ MJ.s/mm² and $\omega = -2$ MJ/mm². The other parameters $E_u =$
 70×10^3 MPa, $\varepsilon = 2$ mm and $R_0 = 0$, are taken as in the previous study.

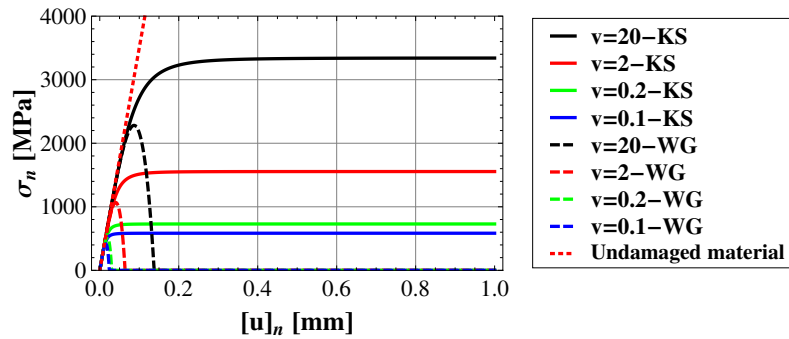


Fig. 8: Interface law for a ramp displacement jump: parametric study on the loading rate v . Kachanov-Sevostianov (KS, solid lines) and Welemane-Goidescu (WG, dashed lines) damaged material models are represented. The linear-elastic behavior of the undamaged material is represented with a red dotted line.

346

347 Figure 8 shows the interface law in the case of the ramp displacement
 348 jump. In analogy with the previous section, a ductile damage behavior of the
 349 interface is obtained in the case of **KS model** and a brittle damage behavior
 350 for **WG model**.

351

352 Figure 9 shows the interface law in the case of the quadratic displacement
 jump. The imposed quadratic displacement jump produces an hardening-like

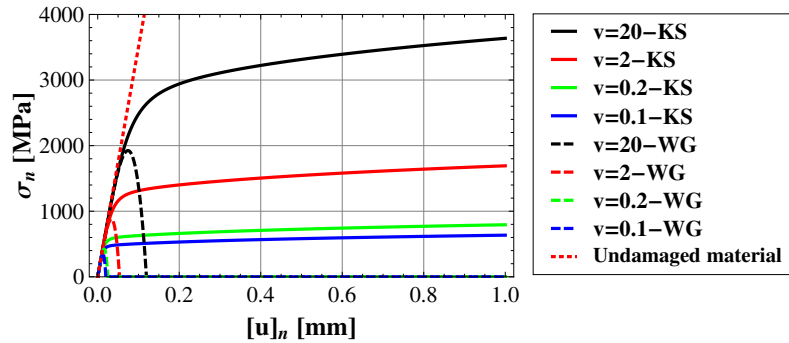


Fig. 9: Interface law for a quadratic displacement-jump: parametric study on the loading rate v . Kachanov-Sevostianov (KS, solid lines) and Welemane-Goidescu (WG, dashed lines) damaged material models are represented. The linear-elastic behavior of the undamaged material is represented with a red dotted line.

353 effect in the damaged part of the interface constitutive behavior (*i.e.*, beyond
 354 the elastic limit) and the slope increases with the loading rate v .

355 Both Figs. 8-9 highlight that for high-rates ($v = 2, 20$ mm/s) the elastic
 356 limit (tensile) is higher than in the quasi-static configurations ($v = 0.1, 0.2$
 357 mm/s) for both KS and WG models. Recently, authors provide a validation
 358 of the proposed hard interface model in [31], by comparing simulated response
 359 curves with data from tensile experimental tests available in the literature
 360 [56] in both quasi-static and high-rate loading conditions. They found that
 361 the loading-rate dependence of the hard interface model makes it suitable to
 362 describe the experimental behavior observed in [56].

363 4.1.3. Effects of cyclic loading

364 The influence of cyclic loading on the hard interface model has also been
 365 investigated. A strictly positive sinusoidal displacement jump has been im-

366 posed: $[u]_n = [u]_{max} |\sin(f t/t_f)|$, with $[u]_{max} = 1$ mm, $f = \pi/2$, $t_f = 5$ s
 367 and 5 cycles have been considered. Both KS and WG damage models have
 368 been considered and the damage parameters have been taken equal to their
 369 reference values $\eta = 30$ MJ.s/mm² and $\omega = -2$ MJ/mm². $E_u = 70 \times 10^3$
 MPa, $\varepsilon = 2$ mm and $R_0 = 0$, as in the previous study.

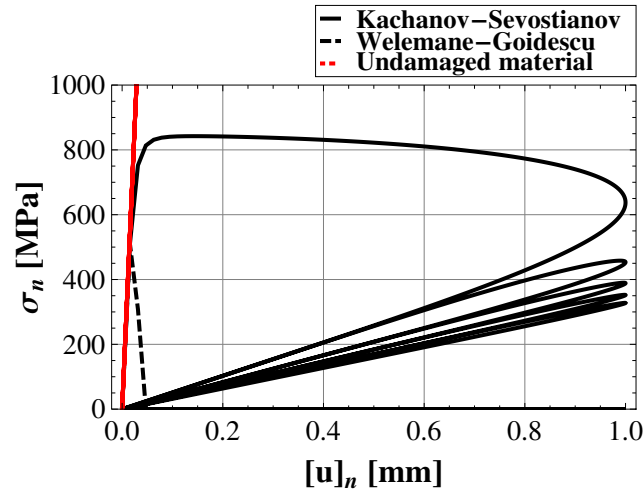


Fig. 10: Interface law for a cyclic load for KS and WG model. The linear-elastic behavior of the undamaged material is represented with a red dotted line.

370

371 As shown in Fig. 10, the two damage models give very different results
 372 under the same loading and parameter conditions. **KS model**, together with
 373 the proposed damage evolution law, is able to reproduce an elastic-damaged
 374 material behavior with hysteresis, as illustrated in Fig. 10. Generally, the en-
 375 ergy dissipated via micro-cracking damage is higher at the initiation and first
 376 accumulation of microcracks. This is consistent with the resulting hysteresis
 377 loop of the first cycle that is larger than the others; after the first cycle, the

378 hysteresis decreases with the number of cycles until the damage evolution
 379 is completed. Moreover, the damage evolution produces a decreasing of the
 380 interface stiffness (see Fig. 10). The stiffness of the undamaged material is
 381 equal to 35000 N/mm^3 and after the first cycle it reduces to 515 N/mm^3 .
 382 After the first reloading (2nd cycle), the stiffness slightly decreases until the
 383 damage evolution is completed, and at the end of the fifth cycle the stiffness
 384 is equal to 318 N/mm^3 . This result is physically plausible.

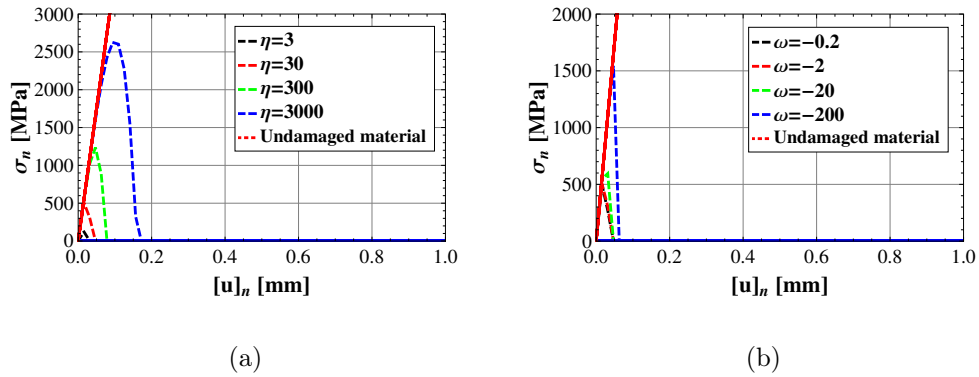


Fig. 11: Interface law for a cyclic load for WG model. Fig. 11(a): study on η .
 Fig. 11(b): study on ω .

385 On the contrary, **WG** damage model is not able to reproduce a damage
 386 behavior under cyclic loads. Figure 10 shows an abrupt reduction in stiffness
 387 to zero already during the first loading curve, meaning that the damaged
 388 material behavior is brittle, in agreement with the previous results. Note
 389 that this behavior does not depend on the chosen values of the damaged
 390 parameters η and ω , as illustrated in Fig. 11.

391 Finally, Fig. 12 shows the evolution in time of the normal stress σ_n in the
 392 case of **KS model**, highlighting the decrease of the maximum normal stress

393 with the number of cycles (note a decrease of the 60% at the last cycle).

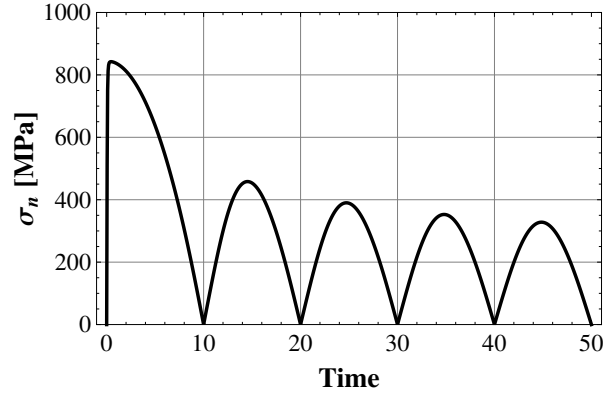


Fig. 12: Interface law for a cyclic load: normal stress as a function of the time for the Kachanov-Sevostianov damage model.

394 *4.2. 1-D example: The structural behavior*

395 In this section, a simple 1-D example is developed to illustrate the struc-
 396 tural behavior of the proposed hard interface model. A composite bar under
 397 traction was considered. The bar, of section A , comprised two parts of length
 398 ℓ , made of an undamaged material with Young's modulus E_u , and an embed-
 399 ded part of length ε , made of a damageable material (glue-like interphase)
 400 with Young's modulus $E_d(E_u, R)$. The damageable material in the inter-
 401 phase is supposed to have at the beginning the same Young's modulus of the
 402 adherents, then it degrades as the microcracks density R evolves. The bar
 403 was fixed at one end and a quasi-static traction force was $F(t)$ applied on
 404 the other end, as illustrated in Fig. 13.

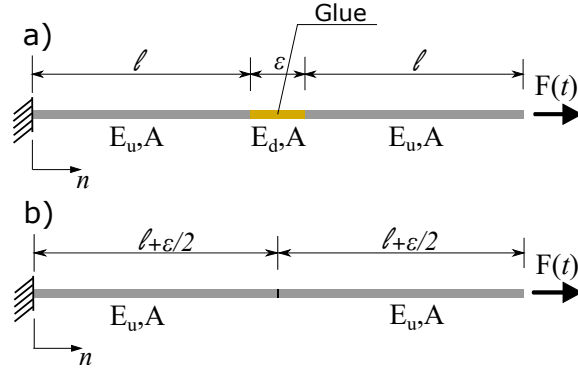


Fig. 13: 1-D example: bar under traction, a) glue interphase, b) interface model

405 The displacement field can be easily derived analytically as:

$$u(n) = \begin{cases} \frac{F}{E_u A} n & 0 \leq n \leq l \\ \frac{F}{E_d A} n + \frac{F l}{A} \left(\frac{1}{E_u} - \frac{1}{E_d} \right) & l \leq n \leq l + \varepsilon \\ \frac{F}{E_u A} n - \frac{F \varepsilon}{A} \left(\frac{1}{E_u} - \frac{1}{E_d} \right) & l + \varepsilon \leq n \leq 2l + \varepsilon \end{cases} \quad (33)$$

406 Thus, the displacement jump along n is obtained as $[u]_n = u(l + \varepsilon) - u(l)$:

$$[u]_n = \frac{F \varepsilon}{E_d A} \quad (34)$$

407 Note that, being $\frac{F}{A} = \sigma_n$, the standard spring-like interface law in 1-D ap-
408 proximation can be derived (in analogy with Eq. (32)).

409 The Young's modulus of the damaged material $E_d(E_u, R)$ was specialized
410 to the case of KS and WG model following Eqs. (29) as in the previous
411 example. The expressions of the evolution of damage Eqs. (31) taking into
412 account the displacement jump Eq. (34) is derived in this 1-D case as:

$$\dot{R} = \begin{cases} \frac{1}{\eta} \left(\omega + \pi \frac{\sigma_n^2}{E_u} \varepsilon \right)_+ & \text{for KS model} \\ \frac{1}{\eta} \left(\omega + \pi \frac{\sigma_n^2}{E_u} \varepsilon \frac{1}{(1 - 2\pi R)^2} \right)_+ & \text{for WG model} \end{cases} \quad (35)$$

413 where $\sigma_n = \bar{\sigma} \bar{t}$ with $\bar{t} = \frac{t}{t_f} \in [0, 1]$, $t_f = 5$ s and $\bar{\sigma} = 400$ MPa. Moreover,
 414 reference values are taken as previously: $E_u = 70 \times 10^3$ MPa, $\varepsilon = 2$ mm,
 415 $\eta = 30$ MJ.s/mm² and $\omega = -2$ MJ/mm².

416 The structural response of the proposed hard interface model, in terms
 417 of tensile stress as a function of the macroscopic displacement jump, is il-
 418 lustrated in Fig. 14, where we find again a brittle behavior for WG material
 and a ductile behavior for KS material.

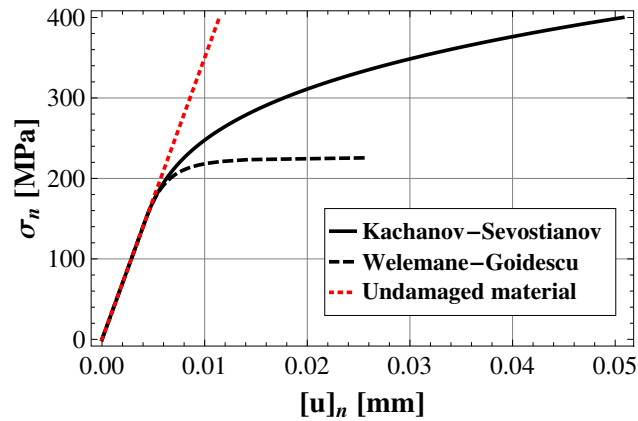


Fig. 14: Interface law in the 1-D case: Kachanov-Sevostianov model (KS, solid line), Welemane-Goidescu model (WG, dashed line), undamaged material (red dotted line).

419

420 5. Conclusions

421 This work proposes an original model of hard imperfect interface account-
 422 ing for micro-cracking and damage evolution. **Preliminary numerical results**
 423 **based on simple academic examples**, in terms of both constitutive and struc-

424 tural behavior, are promising. They suggest that the model could repre-
425 sent a suitable strategy for a macroscopic description of hard adhesives with
426 micro-cracking damage, regardless of whether they have a ductile or brittle
427 behavior. In fact, the analytical interface model could be included in a finite
428 element context via user-defined interface finite elements. Moreover, connec-
429 tion relationships between the generalized cracks density and the standard
430 normalized damage variable, derived at Section 3.3, are expected to simplify
431 the implementation in commercial FEA-software for future validation with
432 numerical simulation.

433 The main perspective to enhance the proposed model is to establish a
434 combined experimental/modelling identification protocol for the damage pa-
435 rameters of the evolution law, the damage viscosity η and the damage thresh-
436 old ω . A design of experience will be set up in order to catch the interactions
437 between damage parameters η and ω that we could only glimpse through the
438 OFAT approach. To this aim, authors have specialized the proposed hard
439 interface model to the case of tubular-butt joints under combined tensile-
440 torsion loads [31]. This is a standard experimental design used to charac-
441 terize structural adhesives and it allows future validations of the proposed
442 interface model with experimental tests.

443 A. Matched asymptotic expansions method

444 A.1. Rescaling phase

445 The rescaling phase of the asymptotic process represents a mathematical
446 construct [46], not a physically-based configuration, and it is used in order to
447 eliminate the dependency of the integration domains on the small parameter

448 ε . This construct can also be seen as a change of spatial variables in the
 449 interphase domain [45, 46] $\hat{\mathbf{p}} := (x_1, x_2, x_3) \rightarrow (z_1, z_2, z_3)$:

$$z_1 = x_1, \quad z_2 = x_2, \quad z_3 = \frac{x_3}{\varepsilon} \quad (\text{A.1})$$

450 resulting

$$\frac{\partial}{\partial z_1} = \frac{\partial}{\partial x_1}, \quad \frac{\partial}{\partial z_2} = \frac{\partial}{\partial x_2}, \quad \frac{\partial}{\partial z_3} = \varepsilon \frac{\partial}{\partial x_3} \quad (\text{A.2})$$

451 as well as in the adherents $\bar{\mathbf{p}} := (x_1, x_2, x_3) \rightarrow (z_1, z_2, z_3)$:

$$z_1 = x_1, \quad z_2 = x_2, \quad z_3 = x_3 \pm \frac{1}{2}(1 - \varepsilon) \quad (\text{A.3})$$

452 where the plus (minus) sign applies whenever $x \in \Omega^{\varepsilon_+}$ ($x \in \Omega^{\varepsilon_-}$), with

$$\frac{\partial}{\partial z_1} = \frac{\partial}{\partial x_1}, \quad \frac{\partial}{\partial z_2} = \frac{\partial}{\partial x_2}, \quad \frac{\partial}{\partial z_3} = \frac{\partial}{\partial x_3} \quad (\text{A.4})$$

453 After the change of variables (A.1) and (A.3), the interphase occupies the
 454 domain $\mathcal{B} = \{(z_1, z_2, z_3) \in \mathbb{R}^3 : (z_1, z_2) \in \mathcal{S}, |z_3| < \frac{1}{2}\}$ and the adherents
 455 occupy the domains $\Omega_{\pm} = \Omega^{\varepsilon_{\pm}} \pm \frac{1}{2}(1 - \varepsilon)\mathbf{i}_3$, as shown in Fig. 2b. The sets
 456 $\mathcal{S}_{\pm} = \{(z_1, z_2, z_3) \in \mathbb{R}^3 : (z_1, z_2) \in \mathcal{S}, z_3 = \pm \frac{1}{2}\}$ are taken to denote the
 457 interfaces between \mathcal{B} and Ω_{\pm} and $\Omega = \Omega_+ \cup \Omega_- \cup \mathcal{B} \cup \mathcal{S}_+ \cup \mathcal{S}_-$ is the rescaled
 458 configuration of the composite body. Γ_u and Γ_g indicate the images of Γ_u^{ε}
 459 and Γ_g^{ε} after the change of variables, and $\bar{\mathbf{f}}^{\pm} := \mathbf{f}^{\pm} \circ \bar{\mathbf{p}}^{-1}$ and $\bar{\mathbf{g}}^{\pm} := \mathbf{g}^{\pm} \circ \bar{\mathbf{p}}^{-1}$
 460 the rescaled external forces.

461 A.2. Kinematic equations

Following the approach proposed in [23, 25], let us focus on the kinematics of the elastic problem. After taking $\hat{\mathbf{u}}^{\varepsilon} = \mathbf{u}^{\varepsilon} \circ \hat{\mathbf{p}}^{-1}$ and $\bar{\mathbf{u}}^{\varepsilon} = \mathbf{u}^{\varepsilon} \circ \bar{\mathbf{p}}^{-1}$ to

denote the displacement fields from the rescaled adhesive and adherents, respectively, the asymptotic expansions of the displacement fields with respect to ε are:

$$\mathbf{u}^\varepsilon(x_1, x_2, x_3) = \mathbf{u}^0 + \varepsilon \mathbf{u}^1 + \varepsilon^2 \mathbf{u}^2 + o(\varepsilon^2) \quad (\text{A.5a})$$

$$\hat{\mathbf{u}}^\varepsilon(z_1, z_2, z_3) = \hat{\mathbf{u}}^0 + \varepsilon \hat{\mathbf{u}}^1 + \varepsilon^2 \hat{\mathbf{u}}^2 + o(\varepsilon^2) \quad (\text{A.5b})$$

$$\bar{\mathbf{u}}^\varepsilon(z_1, z_2, z_3) = \bar{\mathbf{u}}^0 + \varepsilon \bar{\mathbf{u}}^1 + \varepsilon^2 \bar{\mathbf{u}}^2 + o(\varepsilon^2) \quad (\text{A.5c})$$

462 *Interphase.* The gradient of the displacement field $\hat{\mathbf{u}}^\varepsilon$ reads:

$$\nabla(\hat{\mathbf{u}}^\varepsilon) = \varepsilon^{-1} \begin{bmatrix} 0 & \hat{u}_{\alpha,3}^0 \\ 0 & \hat{u}_{3,3}^0 \end{bmatrix} + \begin{bmatrix} \hat{u}_{\alpha,\beta}^0 & \hat{u}_{\alpha,3}^1 \\ \hat{u}_{3,\beta}^0 & \hat{u}_{3,3}^1 \end{bmatrix} + \varepsilon \begin{bmatrix} \hat{u}_{\alpha,\beta}^1 & \hat{u}_{\alpha,3}^2 \\ \hat{u}_{3,\beta}^1 & \hat{u}_{3,3}^2 \end{bmatrix} + O(\varepsilon^2) \quad (\text{A.6})$$

463 where $\alpha, \beta = 1, 2$, so that the strain tensor is:

$$\mathbf{e}(\hat{\mathbf{u}}^\varepsilon) = \frac{1}{2} \left[\nabla(\hat{\mathbf{u}}^\varepsilon) + \nabla(\hat{\mathbf{u}}^\varepsilon)^T \right] = \varepsilon^{-1} \hat{\mathbf{e}}^{-1} + \hat{\mathbf{e}}^0 + \varepsilon \hat{\mathbf{e}}^1 + O(\varepsilon^2) \quad (\text{A.7})$$

464 with:

$$\hat{\mathbf{e}}^{-1} = \begin{bmatrix} 0 & \frac{1}{2} \hat{u}_{\alpha,3}^0 \\ \frac{1}{2} \hat{u}_{\alpha,3}^0 & \hat{u}_{3,3}^0 \end{bmatrix} = \text{Sym}(\hat{\mathbf{u}}_{,3}^0 \otimes \mathbf{i}_3) \quad (\text{A.8})$$

$$\hat{\mathbf{e}}^k = \begin{bmatrix} \text{Sym}(\hat{u}_{\alpha,\beta}^k) & \frac{1}{2}(\hat{u}_{3,\alpha}^k + \hat{u}_{\alpha,3}^{k+1}) \\ \frac{1}{2}(\hat{u}_{3,\alpha}^k + \hat{u}_{\alpha,3}^{k+1}) & \hat{u}_{3,3}^{k+1} \end{bmatrix} = \text{Sym}(\hat{\mathbf{u}}_{,1}^k \otimes \mathbf{i}_1 + \hat{\mathbf{u}}_{,2}^k \otimes \mathbf{i}_2 + \hat{\mathbf{u}}_{,3}^{k+1} \otimes \mathbf{i}_3) \quad (\text{A.9})$$

465 where $\text{Sym}(\cdot)$ gives the symmetric part of the enclosed tensor and $k = 0, 1$,

466 and \otimes is the dyadic product between vectors such as: $(\mathbf{a} \otimes \mathbf{b})_{ij} = a_i b_j$.

467 Moreover, the following notation for derivatives is adopted: $f_{,j}$ denoting the

468 partial derivative of f with respect to z_j .

469 *Adherents.* The gradient of the displacement field $\bar{\mathbf{u}}^\varepsilon$ reads:

$$\nabla(\bar{\mathbf{u}}^\varepsilon) = \begin{bmatrix} \bar{u}_{\alpha,\beta}^0 & \bar{u}_{\alpha,3}^0 \\ \bar{u}_{3,\beta}^0 & \bar{u}_{3,3}^0 \end{bmatrix} + \varepsilon \begin{bmatrix} \bar{u}_{\alpha,\beta}^1 & \bar{u}_{\alpha,3}^1 \\ \bar{u}_{3,\beta}^1 & \bar{u}_{3,3}^1 \end{bmatrix} + O(\varepsilon^2) \quad (\text{A.10})$$

470 so that the strain tensor is:

$$\mathbf{e}(\bar{\mathbf{u}}^\varepsilon) = \frac{1}{2} \left[\nabla(\bar{\mathbf{u}}^\varepsilon) + \nabla(\bar{\mathbf{u}}^\varepsilon)^T \right] = \varepsilon^{-1} \bar{\mathbf{e}}^{-1} + \bar{\mathbf{e}}^0 + \varepsilon \bar{\mathbf{e}}^1 + O(\varepsilon^2) \quad (\text{A.11})$$

471 with:

$$\bar{\mathbf{e}}^{-1} = \mathbf{0} \quad (\text{A.12})$$

472

$$\bar{\mathbf{e}}^k = \begin{bmatrix} \text{Sym}(\bar{u}_{\alpha,\beta}^k) & \frac{1}{2}(\bar{u}_{3,\alpha}^k + \bar{u}_{\alpha,3}^k) \\ \frac{1}{2}(\bar{u}_{3,\alpha}^k + \bar{u}_{\alpha,3}^k) & \bar{u}_{3,3}^k \end{bmatrix} = \text{Sym}(\bar{\mathbf{u}}_{,1}^k \otimes \mathbf{i}_1 + \bar{\mathbf{u}}_{,2}^k \otimes \mathbf{i}_2 + \bar{\mathbf{u}}_{,3}^k \otimes \mathbf{i}_3) \quad (\text{A.13})$$

473 and $k = 0, 1$.

474 A.3. Equilibrium equations

The stress fields in the rescaled adhesive and adherents, $\hat{\boldsymbol{\sigma}}^\varepsilon = \boldsymbol{\sigma} \circ \hat{\mathbf{p}}^{-1}$ and $\bar{\boldsymbol{\sigma}}^\varepsilon = \boldsymbol{\sigma} \circ \bar{\mathbf{p}}^{-1}$ respectively, can be represented as asymptotic expansions [23, 25]:

$$\boldsymbol{\sigma}^\varepsilon = \boldsymbol{\sigma}^0 + \varepsilon \boldsymbol{\sigma}^1 + O(\varepsilon^2) \quad (\text{A.14a})$$

$$\hat{\boldsymbol{\sigma}}^\varepsilon = \hat{\boldsymbol{\sigma}}^0 + \varepsilon \hat{\boldsymbol{\sigma}}^1 + O(\varepsilon^2) \quad (\text{A.14b})$$

$$\bar{\boldsymbol{\sigma}}^\varepsilon = \bar{\boldsymbol{\sigma}}^0 + \varepsilon \bar{\boldsymbol{\sigma}}^1 + O(\varepsilon^2) \quad (\text{A.14c})$$

475 *Interphase.* As body forces are neglected, the equilibrium equation is:

$$\text{div} \hat{\boldsymbol{\sigma}}^\varepsilon = \mathbf{0} \quad (\text{A.15})$$

476 Substituting Eq. (A.14b) in Eq. (A.15) and using Eq. (A.2), it becomes:

$$\begin{aligned} 0 &= \hat{\sigma}_{i\alpha,\alpha}^\varepsilon + \varepsilon^{-1} \hat{\sigma}_{i3,3}^\varepsilon \\ &= \varepsilon^{-1} \hat{\sigma}_{i3,3}^0 + \hat{\sigma}_{i\alpha,\alpha}^0 + \hat{\sigma}_{i3,3}^1 + \varepsilon \hat{\sigma}_{i\alpha,\alpha}^1 + O(\varepsilon) \end{aligned} \quad (\text{A.16})$$

477 where $\alpha = 1, 2$. Eq. (A.16) has to be satisfied for any value of ε , leading to:

$$\hat{\sigma}_{i3,3}^0 = 0 \quad (\text{A.17})$$

$$\hat{\sigma}_{i1,1}^0 + \hat{\sigma}_{i2,2}^0 + \hat{\sigma}_{i3,3}^1 = 0 \quad (\text{A.18})$$

478 where $i = 1, 2, 3$.

479 Eq. (A.17) shows that $\hat{\sigma}_{i3}^0$ is not dependent on z_3 in the adhesive, and
480 thus it can be written:

$$[\hat{\sigma}_{i3}^0] = 0 \quad (\text{A.19})$$

481 where $[\cdot]$ denotes the jump between $z_3 = \frac{1}{2}$ and $z_3 = -\frac{1}{2}$. In view of
482 Eq. (A.19), Eq. (A.18), for $i = 3$, can be rewritten in the integrated form

$$[\hat{\sigma}_{33}^1] = -\hat{\sigma}_{13,1}^0 - \hat{\sigma}_{23,2}^0 \quad (\text{A.20})$$

483 *Adherents.* The equilibrium equation in the adherents is:

$$\text{div} \bar{\boldsymbol{\sigma}}^\varepsilon + \bar{\mathbf{f}} = \mathbf{0} \quad (\text{A.21})$$

484 Substituting Eq. (A.14c) in Eq. (A.21) that has to be satisfied for any value
485 of ε , leads to:

$$\text{div} \bar{\boldsymbol{\sigma}}^0 + \bar{\mathbf{f}} = \mathbf{0} \quad (\text{A.22})$$

$$\text{div} \bar{\boldsymbol{\sigma}}^1 = \mathbf{0} \quad (\text{A.23})$$

486 *A.4. Matching phase*

487 The imposed continuity conditions at $\mathcal{S}_{\pm}^{\varepsilon}$ for the fields \mathbf{u}^{ε} and $\boldsymbol{\sigma}^{\varepsilon}$ lead to
 488 matching relationships between external and internal expansions [23, 25]. In
 489 terms of displacements the following relationship have to be satisfied:

$$\mathbf{u}^{\varepsilon}(\mathbf{x}_{\alpha}, \pm \frac{\varepsilon}{2}) = \hat{\mathbf{u}}^{\varepsilon}(\mathbf{z}_{\alpha}, \pm \frac{1}{2}) = \bar{\mathbf{u}}^{\varepsilon}(\mathbf{z}_{\alpha}, \pm \frac{1}{2}) \quad (\text{A.24})$$

490 where $\mathbf{x}_{\alpha} := (x_1, x_2)$, $\mathbf{z}_{\alpha} := (z_1, z_2) \in \mathcal{S}$. Expanding the displacement in the
 491 adherents \mathbf{u}^{ε} , in Taylor series along the x_3 -direction and taking into account
 492 Eq. (A.5a), it results:

$$\begin{aligned} \mathbf{u}^{\varepsilon}(\mathbf{x}_{\alpha}, \pm \frac{\varepsilon}{2}) &= \mathbf{u}^{\varepsilon}(\mathbf{x}_{\alpha}, 0^{\pm}) \pm \frac{\varepsilon}{2} \mathbf{u}_{,3}^{\varepsilon}(\mathbf{x}_{\alpha}, 0^{\pm}) + \dots \\ &= \mathbf{u}^0(\mathbf{x}_{\alpha}, 0^{\pm}) + \varepsilon \mathbf{u}^1(\mathbf{x}_{\alpha}, 0^{\pm}) \pm \frac{\varepsilon}{2} \mathbf{u}_{,3}^0(\mathbf{x}_{\alpha}, 0^{\pm}) + \dots \end{aligned} \quad (\text{A.25})$$

493 Substituting Eqs. (A.5b) and (A.5c) together with Eq. (A.25) in Eq. (A.24),
 494 it holds true:

$$\begin{aligned} &\mathbf{u}^0(\mathbf{x}_{\alpha}, 0^{\pm}) + \\ &+ \varepsilon \mathbf{u}^1(\mathbf{x}_{\alpha}, 0^{\pm}) \pm \frac{\varepsilon}{2} \mathbf{u}_{,3}^0(\mathbf{x}_{\alpha}, 0^{\pm}) + \dots = \hat{\mathbf{u}}^0(\mathbf{z}_{\alpha}, \pm \frac{1}{2}) + \varepsilon \hat{\mathbf{u}}^1(\mathbf{z}_{\alpha}, \pm \frac{1}{2}) + \dots \\ &= \bar{\mathbf{u}}^0(\mathbf{z}_{\alpha}, \pm \frac{1}{2}) + \varepsilon \bar{\mathbf{u}}^1(\mathbf{z}_{\alpha}, \pm \frac{1}{2}) + \dots \end{aligned} \quad (\text{A.26})$$

495 By identifying the terms in the same powers of ε , Eq. (A.26) gives:

$$\mathbf{u}^0(\mathbf{x}_{\alpha}, 0^{\pm}) = \hat{\mathbf{u}}^0(\mathbf{z}_{\alpha}, \pm \frac{1}{2}) = \bar{\mathbf{u}}^0(\mathbf{z}_{\alpha}, \pm \frac{1}{2}) \quad (\text{A.27})$$

$$\mathbf{u}^1(\mathbf{x}_{\alpha}, 0^{\pm}) \pm \frac{1}{2} \mathbf{u}_{,3}^0(\mathbf{x}_{\alpha}, 0^{\pm}) = \hat{\mathbf{u}}^1(\mathbf{z}_{\alpha}, \pm \frac{1}{2}) = \bar{\mathbf{u}}^1(\mathbf{z}_{\alpha}, \pm \frac{1}{2}) \quad (\text{A.28})$$

496 By identification process, analogous results are obtained in terms of stresses
 497 [23, 25]:

$$\sigma_{i3}^0(\mathbf{x}_{\alpha}, 0^{\pm}) = \hat{\sigma}_{i3}^0(\mathbf{z}_{\alpha}, \pm \frac{1}{2}) = \bar{\sigma}_{i3}^0(\mathbf{z}_{\alpha}, \pm \frac{1}{2}) \quad (\text{A.29})$$

$$\sigma_{i3}^1(\mathbf{x}_\alpha, 0^\pm) \pm \frac{1}{2}\sigma_{i3,3}^0(\mathbf{x}_\alpha, 0^\pm) = \hat{\sigma}_{i3}^1(\mathbf{z}_\alpha, \pm\frac{1}{2}) = \bar{\sigma}_{i3}^1(\mathbf{z}_\alpha, \pm\frac{1}{2}) \quad (\text{A.30})$$

for $i = 1, 2, 3$.

A.5. Constitutive equations

The constitutive laws in linear elasticity for the adherents and the interphase are considered:

$$\bar{\boldsymbol{\sigma}}^\varepsilon = \mathbb{A}_\pm(\mathbf{e}(\bar{\mathbf{u}}^\varepsilon)) \quad (\text{A.31a})$$

$$\hat{\boldsymbol{\sigma}}^\varepsilon = \mathbb{B}^\varepsilon(\mathbf{e}(\hat{\mathbf{u}}^\varepsilon)) \quad (\text{A.31b})$$

where $\mathbb{A}_\pm, \mathbb{B}^\varepsilon$ are the elasticity tensor of adherents and of interphase, respectively.

Funding: This work has been supported by the University of Ferrara via FAR grants 2020 and 2021.

References

- [1] Sekiguchi, Y., Sato, C. (2021) *Experimental investigation of the effects of adhesive thickness on the fracture behavior of structural acrylic adhesive joints under various loading rates*, Int. J. Adhes. Adhes., 105:102782.
- [2] Miao, C., Fernando, D., Heitzmann, M. T., Bailleres, H. (2019) *GFRP-to-timber bonded joints: Adhesive selection*, Int. J. Adhes. Adhes., 94:29-39.

- 513 [3] Yamamoto, A., Yoshida, T., Tsubota, K., Takamizawa, T., Kurokawa,
514 H., Miyazaki, M. (2006) *Orthodontic bracket bonding: enamel bond*
515 *strength vs time*, Am. J. Orthod. Dentofacial Orth., 130(4):435-e1.
- 516 [4] Benveniste, Y. and Miloh, T. (2001) *Imperfect soft and stiff interfaces*
517 *in two-dimensional elasticity*, Mech. Mat., 33 (6):309–323
- 518 [5] Hashin, Z. (2002) *Thin interphase/imperfect interface in elasticity with*
519 *application to coated fiber composites*, J. Mech. Phys. Solid, 50(12):2509–
520 2537.
- 521 [6] Frémond, M. (1987) *Adhesion of solids*, J. Mech. Th. Appl., 6(3):383–
522 407.
- 523 [7] Bonetti E., Bonfanti G., Lebon F., Rizzoni, R. (2017) *A model of im-*
524 *perfect interface with damage*, Meccanica, 52(8):1911–1922
- 525 [8] Raous, M., Cangemi, L., Cocu, M. (1999) *A consistent model coupling*
526 *adhesion, friction, and unilateral contact*, Comput. Meth. Appl. Mech.
527 Eng., 177(3-4):383–399.
- 528 [9] Del Piero, G., Raous, M. (2010) *A unified model for adhesive interfaces*
529 *with damage, viscosity, and friction*, Eur. J. Mech.-A/Solid, 29(4):496–
530 507.
- 531 [10] Freddi, F., Frémond, M. (2006) *Damage in domains and interfaces: a*
532 *coupled predictive theory*, J. Mech. Mat. Struct., 1(7):1205-1233.
- 533 [11] Raffa, M.L., Lebon, F., Rizzoni R. (2016) *On modelling brick/mortar*

- 534 *interface via a St. Venant-Kirchhoff orthotropic soft interface. Part I:*
535 *theory*, Int. J. Masonry Res. Innov., 1 (2):142-164.
- 536 [12] Dumont, S., Lebon, F., Raffa, M. L., Rizzoni, R. (2017) *Towards nonlin-*
537 *ear imperfect interface models including micro-cracks and smooth rough-*
538 *ness*, Annal Solid Struct. Mech., 9(1-2):13–27.
- 539 [13] Raffa, M.L., Lebon, F., Rizzoni R. (2017) *On modelling brick/mortar*
540 *interface via a St. Venant-Kirchhoff orthotropic soft interface. Part II:*
541 *in silico analysis*, Int. J. Masonry Res. Innov., 2(4):259-273.
- 542 [14] Raffa, M. L., Lebon, F., Rizzoni, R. (2018) *Derivation of a model of im-*
543 *perfect interface with finite strains and damage by asymptotic techniques:*
544 *an application to masonry structures*, Meccanica, 53(7):1645-1660.
- 545 [15] Maurel-Pantel, A., Lamberti, M., Raffa, M. L., Suarez, C., Ascione, F.,
546 Lebon, F. (2020) *Modelling of a GFRP adhesive connection by an imper-*
547 *fect soft interface model with initial damage*, Comp. Struct., 239:112034.
- 548 [16] Needleman, A. (1990) *An analysis of tensile decohesion along an inter-*
549 *face*, J. Mech. Phys. Solid, 38(3):289-324.
- 550 [17] Costanzo, F. (1998) *A continuum theory of cohesive zone models: defor-*
551 *mation and constitutive equations*, Int. J. Engng. Sci., 36(15):1763-1792.
- 552 [18] Alfano G., Sacco E. (2006) *Combining interface damage and friction in*
553 *a cohesive-zone model*, Int. J. Numer. Meth. Engng. 68 (5):542–582
- 554 [19] Chen, P., Chen, S., Peng, J. (2016) *Interface behavior of a thin-film*

- 555 *bonded to a graded layer coated elastic half-plane*, Int. J. Mech. Sci.
556 115:489-500.
- 557 [20] Chen, P., Peng, J., Chen, Z., Peng, G. (2019) *On the interfacial behavior*
558 *of a piezoelectric actuator bonded to a homogeneous half plane with an*
559 *arbitrarily varying graded coating*, Eng. Fract. Mech. 220:106645.
- 560 [21] Guo, W., Chen, P., Yu, L., Peng, G., Zhao, Y., Gao, F. (2020) *Numerical*
561 *analysis of the strength and interfacial behaviour of adhesively bonded*
562 *joints with varying bondline thicknesses*, Int. J. Adhes. Adhes. 98:102553.
563
- 564 [22] Chen, P., Chen, S., Liu, H., Peng, J., Gao, F. (2020) *The interface behav-*
565 *ior of multiple piezoelectric films attaching to a finite-thickness gradient*
566 *substrate* J. Appl. Mech.-Trans. ASME, 87(1):011003.
- 567 [23] Lebon, F., Rizzoni, R. (2010) *Asymptotic analysis of a thin interface:*
568 *The case involving similar rigidity*, Int. J. Engng. Sci., 48:473–486
- 569 [24] Lebon, F., Rizzoni, R. (2011) *Asymptotic behavior of a hard thin linear*
570 *elastic interphase: An energy approach*, Int. J. Solid Struct., 48:441–449
- 571 [25] Rizzoni, R., Dumont, S., Lebon, F., Sacco, S. (2014) *Higher order model*
572 *for soft and hard interfaces*, Int. J. Solid Struct., 51:4137-4148
- 573 [26] Dumont, S., Rizzoni, R., Lebon, F., Sacco, E. (2018) *Soft and hard*
574 *interface models for bonded elements*, Comp. Part B: Engng., 153:480–
575 490.

- 576 [27] Furtsev, A., Rudoy, E. (2020) *Variational approach to modelling soft*
577 *and stiff interfaces in the Kirchhoff-Love theory of plates*, Int. J. Solid
578 Struct., 202:562–574.
- 579 [28] Rudoy, E., Shcherbakov, V. (2020) *First-order shape derivative of the*
580 *energy for elastic plates with rigid inclusions and interfacial cracks* Appl.
581 Math. Optim., 1-28.
- 582 [29] Baranova, S., Mogilevskaya, S. G., Nguyen, T. H., Schillinger, D. (2020)
583 *Higher-order imperfect interface modelling via complex variables based*
584 *asymptotic analysis*, Int. J. Engng. Sci., 157:103399.
- 585 [30] Raffa, M.L., Lebon, F., Vairo, G. (2016) *Normal and tangential stiff-*
586 *nesses of rough surfaces in contact via an imperfect interface model*, Int.
587 J. Solid Struct., 87:245-253.
- 588 [31] Raffa, M. L., Rizzoni, R., Lebon, F. (2021) *A Model of Damage for Brit-*
589 *tle and Ductile Adhesives in Glued Butt Joints*, Technologies, 9(1):19.
- 590 [32] Kachanov, M., (1994) *Elastic solids with many cracks and related prob-*
591 *lems*, Adv. Appl. Mech., 30:259–445.
- 592 [33] Mauge C., Kachanov M. (1994) *Effective elastic properties of an*
593 *anisotropic material with arbitrarily oriented interacting cracks*, J. Mech.
594 Phys. Solid, 42:561–584.
- 595 [34] Tsukrov, I., Kachanov, M. (2000) *Effective moduli of an anisotropic*
596 *material with elliptical holes of arbitrary orientational distribution*, Int.
597 J. Solid Struct., 37 (41):5919-5941.

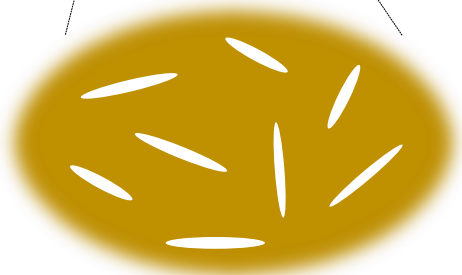
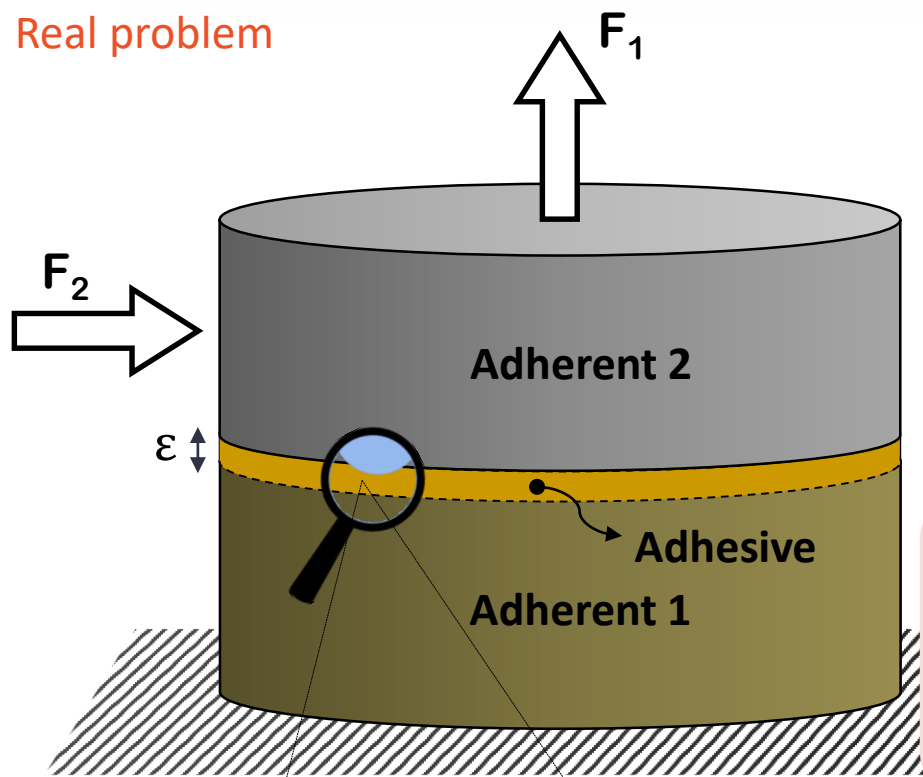
- 598 [35] Kachanov, M., Sevostianov, I. (2005) *On quantitative characterization of*
599 *microstructures and effective properties*, Int. J. Solid Struct., 42(2):309-
600 336.
- 601 [36] Sevostianov, I., Kachanov, M. (2014) *On some controversial issues in*
602 *effective field approaches to the problem of the overall elastic properties*,
603 Mech. Mat., 69:93-105.
- 604 [37] Kachanov, M., Sevostianov, I. (2018) *Micromechanics of materials, with*
605 *applications*, (Vol. 249), Cham: Springer.
- 606 [38] Bruno, G., Kachanov, M., Sevostianov, I., Shyam, A. (2019) *Microme-*
607 *chanical modelling of non-linear stress-strain behavior of polycrystalline*
608 *microcracked materials under tension*, Acta Materialia, 164:50-59.
- 609 [39] Andrieux, S., Bamberger, Y., Marigo, J. J. (1986) *Un modèle de*
610 *matériau microfissuré pour les bétons et les roches*, J. Méc. Théor. Appl,
611 5(3)47:1-513.
- 612 [40] Welemane, H., Goidescu, C. (2010) *Isotropic brittle damage and unilat-*
613 *eral effect*, Compte Rendu Méc., 338(5):271-276.
- 614 [41] Sanchez-Palencia, E. (1980) *Non homogeneous materials and vibration*
615 *theory*, Lecture Notes in Physics, Springer, Berlin, 127.
- 616 [42] Hubert, J. S., Palencia, E. S. (1992) *Introduction aux méthodes asymp-*
617 *totiques et à l'homogénéisation: application à la mécanique des milieux*
618 *continus*, Masson.

- 619 [43] Klarbring A. (1991) *Derivation of the adhesively bonded joints by the*
620 *asymptotic expansion method*, Int. J. Engng. Sci., 29:493–512.
- 621 [44] Geymonat, G., Krasucki, F., Lenci, S. (1999) *Mathematical analysis of*
622 *a bonded joint with a soft thin adhesive*, Math. Mech. Solid, 16:201–225.
- 623 [45] Schmidt, P. (2008) *Modelling of adhesively bonded joints by an asymp-*
624 *totic method*, Int. J. Engng. Sci., 46(12):1291-1324.
- 625 [46] Ciarlet P.G. (1988) *Mathematical Elasticity. Volume I: Three-*
626 *Dimensional Elasticity*, North-Holland, Amsterdam.
- 627 [47] Serpilli, M., Lenci, S. (2008) *Limit models in the analysis of three dif-*
628 *ferent layered elastic strips*, Eur. J.Mech.-A/Solid, 27(2):247-268.
- 629 [48] Serpilli, M., Lenci, S. (2016) *An overview of different asymptotic models*
630 *for anisotropic three-layer plates with soft adhesive*, Int. J. Solid Struct.,
631 81:130-140.
- 632 [49] Goidescu, C., Weleman, H., Kondo, D., Gruescu, C. (2013) *Microcracks*
633 *closure effects in initially orthotropic materials*, Eur. J.Mech.-A/Solid,
634 37:172-184.
- 635 [50] Goidescu, C., Weleman, H., Pantalé, O., Karama, M., Kondo,
636 D. (2015) *Anisotropic unilateral damage with initial orthotropy: A*
637 *micromechanics-based approach*, Int. J. Damage Mech., 24(3):313-337.
- 638 [51] Eshelby, J. D. (1961) *Progress in solid mechanics*, J. Mech. Phys. Solid,
639 9(1):67-67.

- 640 [52] Welemene, H., Cormery, F. (2002) *Some remarks on the damage unilat-*
641 *eral effect modelling for microcracked materials*, Int. J. Damage Mech.,
642 11(1):65-86.
- 643 [53] Frémond, M., Nedjar, B. (1996) *Damage, gradient of damage and prin-*
644 *ciple of virtual power*, Int. J. Solid Struct., 33(8):1083-1103.
- 645 [54] Chaboche, J. L. (1988) *Continuum damage mechanics: Part I—General*
646 *concepts*, J. Appl. Mech., 55:59-64.
- 647 [55] Wolfram Research, Inc. *Mathematica*; Version 12.2; Wolfram Research,
648 Inc.: Champaign, IL, USA, 2020.
- 649 [56] Murakami, S., Sekiguchi, Y., Sato, C., Yokoi, E., Furusawa, T. (2016)
650 *Strength of cylindrical butt joints bonded with epoxy adhesives under*
651 *combined static or high-rate loading*, Int. J. Adhes. Adhes., 67:86–93.

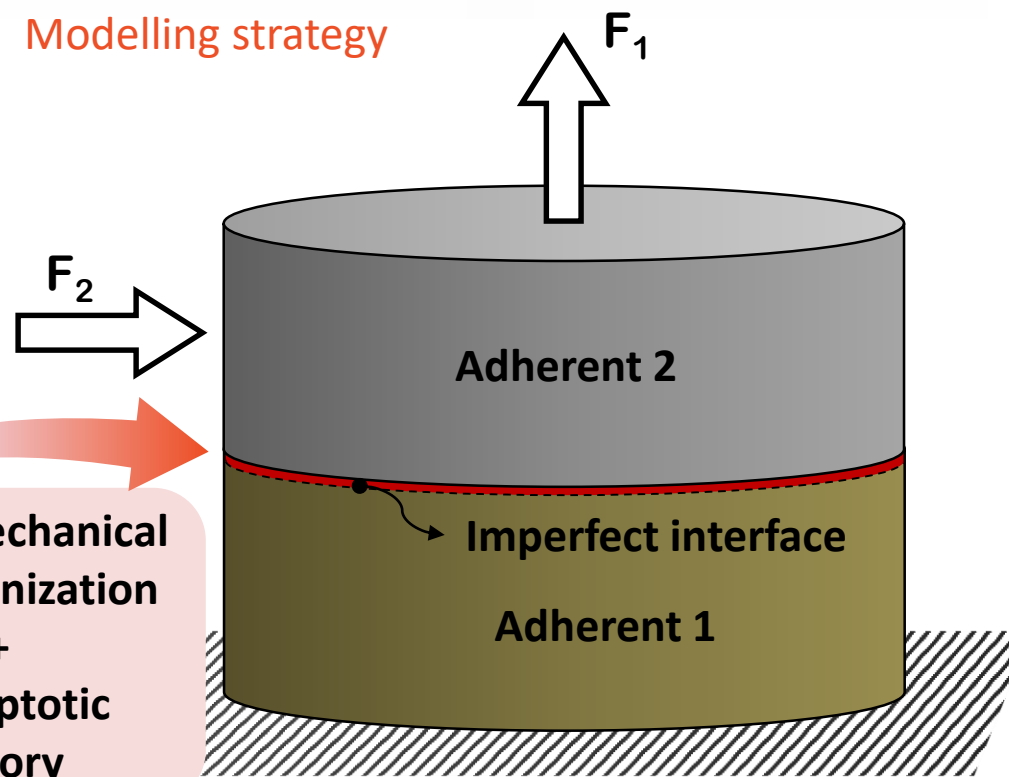
A micromechanical model of a hard interface with micro-cracking damage

Real problem



Micro-cracking damage R

Modelling strategy



Micromechanical homogenization + Asymptotic theory

Hard imperfect interface
 $[[\sigma \cdot n]] \neq 0 \quad [[u]] \neq 0$
 with evolutive damage
 \dot{R}